Available online at www.sciencedirect.com
ScienceDirect
Geochimica et Cosmochimica Acta 71 (2007) 417–433
Geochimica
www.elsevier.com/locate/gca

The experimental calibration of the iron isotope fractionation factor between pyrrhotite and peralkaline rhyolitic melt

Jan A. Schuessler *, Ronny Schoenberg, Harald Behrens, Friedhelm von Blanckenburg

Institut für Mineralogie, Universität Hannover, Callinstr. 3, D-30167 Hannover, Germany

Received 8 December 2005; accepted in revised form 15 September 2006

Abstract

A first experimental study was conducted to determine the equilibrium iron isotope fractionation between pyrrhotite and silicate melt at magmatic conditions. Experiments were performed in an internally heated gas pressure vessel at 500 MPa and temperatures between 840 and 1000 °C for 120–168 h. Three different types of experiments were conducted and after phase separation the iron isotope composition of the run products was measured by MC-ICP-MS. (i) Kinetic experiments using ^{57}Fe-enriched glass and natural pyrrhotite revealed that a close approach to equilibrium is attained already after 48 h. (ii) Isotope exchange experiments—using mixtures of hydrous peralkaline rhyolitic glass powder (~4 wt% H_2O) and natural pyrrhotites ($Fe_{1-x}S$) as starting materials— and (iii) crystallisation experiments, in which pyrrhotite was formed by reaction between elemental sulphur and rhyolitic melt, consistently showed that pyrrhotite preferentially incorporates light iron. No temperature dependence of the fractionation factor was found between 840 and 1000 °C, within experimental and analytical precision. An average fractionation factor of $\Delta\,^{56}Fe/^{54}Fe_{pyrrhotite\text{-}melt} = -0.35 \pm 0.04‰$ (2SE, $n = 13$) was determined for this temperature range. Predictions of Fe isotope fractionation between FeS and ferric iron-dominated silicate minerals are consistent with our experimental results, indicating that the marked contrast in both ligand and redox state of iron control the isotope fractionation between pyrrhotite and silicate melt. Consequently, the fractionation factor determined in this study is representative for the specific $Fe^{2+}/\Sigma Fe$ ratio of our peralkaline rhyolitic melt of 0.38 ± 0.02. At higher $Fe^{2+}/\Sigma Fe$ ratios a smaller fractionation factor is expected. Further investigation on Fe isotope fractionation between other mineral phases and silicate melts is needed, but the presented experimental results already suggest that even at high temperatures resolvable variations in the Fe isotope composition can be generated by equilibrium isotope fractionation in natural magmatic systems.

1. Introduction

The range in iron isotope composition observed in nature cover about 4‰ in $^{56}Fe/^{54}Fe$. In particular low-temperature processes (<100 °C) show a high variability in Fe isotope composition, whereas bulk igneous rocks comprise a more narrow range of about ± 0.1‰ (2σ) (Beard et al., 2003). However, recent studies observed small but significant differences in Fe isotope compositions between mantle rocks and basalts (Weyer et al., 2005) and some silica-rich granitoids show heavier Fe isotope compositions than mafic rocks (Poitrasson and Freydier, 2005; Dauphas and Rouxel, 2006). At present, the experimental database on low-T Fe isotope fractionation processes is steadily growing, whereas experimental studies on high-temperature Fe isotope fractionation in magmatic systems are still lacking.

Calculations based on Mössbauer spectroscopy data allow predictions of inter-mineral Fe isotope fractionation factors at high temperatures. For example, predicted equilibrium Fe isotope fractionation between clinopyroxene and olivine at 800 °C is +0.15‰ for the $^{56}Fe/^{54}Fe$ ratio (Polyakov and Mineev, 2000). However, iron isotope results of igneous rocks and their interpretations are often controversial. Zhu et al. (2002) and Williams et al. (2005) reported significant differences in the $^{56}Fe/^{54}Fe$ ratio of −0.1‰ to −0.2‰ for coexisting olivine and pyroxene in

* Corresponding author. Fax: +49 511 762 3045.
E-mail address: j.schuessler@mineralogie.uni-hannover.de (J.A. Schuessler).

0016-7037/$ - see front matter © 2006 Elsevier Inc. All rights reserved.
doi:10.1016/j.gca.2006.09.012

mantle rocks, but an absence of differences between ortho- and clinopyroxene. The authors suggest that these findings reflect isotopic equilibrium at ~1000 °C. Beard and Johnson (2004) confirmed differences in iron isotopes between coexisting olivine and clinopyroxene for some spinel peridotites, but attributed these to metasomatic alteration. On the other hand, these authors did not find any significant iron isotope fractionation between olivine and orthopyroxene in the investigated spinel peridotites. So far, the largest inter-mineral fractionation in mafic rocks interpreted as equilibrium fractionation was observed for clinopyroxene and garnet in eclogites and in garnet-bearing ultramafic rocks (~+0.3‰ in $^{56}Fe/^{54}Fe$; Beard and Johnson, 2004).

A given mineral phase can show a considerable range in Fe isotope composition depending on the origin of its host rock (Beard and Johnson, 2004; Williams et al., 2004, 2005). The largest variations in $^{56}Fe/^{54}Fe$, up to 1.1‰, were observed for mantle-derived spinels (Williams et al., 2004, 2005). Possible explanations for these variations are melt extraction in combination with changes in mantle-redox conditions or metasomatism of the sub-arc mantle by iron-rich silicate melts from the subducting slab (Williams et al., 2004, 2005). The latter interpretation has already been proposed by Beard and Johnson (2004). In contrast, andesitic volcanic rocks did not reveal any differences in Fe isotope composition between silicate minerals (olivine, biotite, amphibole) and magnetite (Beard and Johnson, 2004).

To date, the mechanisms that cause Fe isotope fractionation in igneous rocks are still poorly understood and experimental calibrations of fractionation factors are missing. The motivation for our study is to clarify whether measurable high-temperature equilibrium Fe isotope fractionation does exist or not. Here, we report a first experimental study on high-temperature iron isotope fractionation under magmatic conditions. We present a detailed study on Fe isotope partitioning between pyrrhotite ($Fe_{1-x}S$) and a hydrous peralkaline rhyolitic melt at temperatures between 840 and 1000 °C and at a pressure of 500 MPa. The pyrrhotite-melt system was chosen mainly because of the experimental simplicity of the system compared to, for example, olivine-melt or pyroxene-melt systems. We have chosen the peralkaline rhyolitic composition for two main reasons. (i) The high FeO content and the relatively low liquidus temperature facilitate experimental and analytical procedures, because pyrrhotite is the only iron-bearing mineral that is stable over a wide temperature range. (ii) The high alkalinity combined with a relatively low Al_2O_3 concentration stabilises ferric over ferrous iron ($Fe^{2+}/\Sigma Fe \sim 0.4$) under our experimental conditions (e.g., Dickenson and Hess, 1986; Mysen, 1988; Gaillard et al., 2001). A pronounced contrast in the oxidation state of iron between the silicate melt and pyrrhotite ($Fe_{1-x}S$ contains almost exclusively ferrous iron), is expected to support iron isotope fractionation (Polyakov and Mineev, 2000; Schauble, 2004). Studies on Fe isotope fractionation between aqueous ferric and ferrous species at low temperatures have shown that the heavier isotope is associated with the higher oxidation state of Fe (Johnson et al., 2002; Welch et al., 2003). Hence, for a first high temperature experimental study the chosen mineral-melt system provides the appropriate boundary conditions, where such predictions can be tested.

2. Experimental methods

Our experimental strategy involves three different experimental designs to distinguish between kinetic and thermodynamic isotope fractionation: (i) The timescale required to attain isotopic equilibrium was determined with experiments using a glass that was artificially enriched in ^{57}Fe and natural pyrrhotite. The large differences in $^{57}Fe/^{54}Fe$ between the starting materials allow precise monitoring of isotope exchange towards equilibrium. (ii) The equilibrium fractionation factors between pyrrhotite and silicate melt were determined by the partial exchange method of Northrop and Clayton (1966). Synthetic glasses and natural pyrrhotites of known Fe isotope compositions were used as starting materials for these experiments. The large variation in Fe isotope composition of the pyrrhotites used allows the determination of fractionation factors even at incomplete equilibration. (iii) In addition, the equilibrium fractionation factor between pyrrhotite and silicate melt was determined by crystallisation experiments in which pyrrhotite was formed by reaction between sulphur and silicate melt.

2.1. Starting materials

2.1.1. Natural pyrrhotite samples

Four different natural pyrrhotites were used in our study. All samples were checked for purity by powder X-ray diffraction (XRD) and electron microprobe analysis (EMPA) (see Table EA-1; all tables and figures with the prefix "EA" refer to the Electronic annex). No phases other than pyrrhotite were detected. In addition no elements other than Fe and S were detected by EMPA. Samples B and K show a single sharp d_{102} peak in the powder X-ray diffraction pattern that indicates hexagonal pyrrhotite. Splitting of this peak as observed for the samples MV and R is characteristic for monoclinic pyrrhotite (Vaughan and Craig, 1978). The $^{56}Fe/^{54}Fe$ ratios of the pyrrhotite samples vary by 0.67‰ (Table 1).

2.1.2. Synthetic peralkaline, rhyolitic glass

As starting glass, we chose a synthetic analogue of a peralkaline rhyolitic obsidian from New Zealand (composition in wt%: 75.5 SiO_2, 10.4 Al_2O_3, 4.1 FeO, 5.3 Na_2O, 4.7 K_2O). The NSLsyn glass was prepared by fusing a mixture of oxides and carbonates at 1600 °C (Table EA-2, NSLsyn dry). In the experiments we used prehydrated glasses as starting materials to assure homogeneous H_2O distribution and to avoid any possible complications due to a fluid

Table 1
Iron isotope compositions of the starting materials

Sample	Analysis No.[a]	δ^{56}Fe	δ^{57}Fe	Averages			
				δ^{56}Fe	2σ[c]	δ^{57}Fe	2σ[c]
Synthetic glasses							
NSLsyn (dry)	NSL1	−0.234	−0.334	−0.247	0.043	−0.346	0.074
	NSL2	−0.276	−0.396				
	NSL3a	−0.252	−0.336				
	NSL3b	−0.282	−0.354				
	NSL4	−0.223	−0.299				
	NSL5a	−0.243	−0.341				
	NSL5b	−0.245	−0.315				
	NSL5c	−0.284	−0.420				
NSLsyn01[b]	NSL6	−0.265	−0.382				
NSLsyn07[b]	NSL7a	−0.225	−0.361				
	NSL7b	−0.225	−0.317				
	NSL7c	−0.231	−0.373				
NSLsyn05[b]	NSL8a	−0.247	−0.330				
	NSL8b	−0.228	−0.289				
$NSLsyn04_{spike}$	NSL9a	0.720	1623.494	0.723	0.043	1623.487	0.364
	NSL9b	0.746	1623.666				
	NSL10	0.704	1623.302				
$NSLsyn06_{spike}$	NSL11a	−0.024	438.092	−0.009	0.025	438.138	0.121
	NSL11b	−0.002	438.206				
	NSL12	−0.002	438.115				
Natural pyrrhotites							
MV	MV1a	−0.733	−1.106	−0.727	0.035	−1.063	0.053
	MV1b	−0.758	−1.079				
	MV2	−0.690	−1.003				
B	B1a	−1.065	−1.554	−1.035	0.037	−1.528	0.078
	B1b	−1.076	−1.589				
	B2a	−1.007	−1.440				
	B2b	−0.991	−1.485				
K	K1a	−0.345	−0.498	−0.369	0.019	−0.526	0.024
	K1b	−0.391	−0.530				
	K2a	−0.366	−0.507				
	K2b	−0.385	−0.558				
	K2c	−0.360	−0.535				
R	R1a	−0.725	−1.077	−0.720	0.011	−1.064	0.015
	R1b	−0.727	−1.057				
	R2a	−0.724	−1.045				
	R2b	−0.704	−1.075				

[a] Each number refers to an analytical sequence involving dissolution of glass or pyrrhotite and chromatographic separation of iron. Characters a, b and c denote multiple Fe isotope analyses of the same solution.
[b] Some of the hydrous glass batches were analysed to ensure that the Fe isotope composition remained unchanged after the hydration procedure.
[c] Uncertainty given as the two standard deviation of replicate analyses. The long-term external reproducibility (2σ) for ''unspiked'' samples on the Neptune mass spectrometer is ±0.049‰ on δ^{56}Fe and ±0.071‰ on δ^{57}Fe.

phase which may initiate metastable reactions in the beginning of the experiment. Details on the preparation of the synthetic glasses are given in the Electronic annex. A H_2O content of ~4 wt% was chosen to obtain a fluid-undersatured melt (Behrens and Jantos, 2001) under the experimental conditions applied here, even in the presence of sulphur. The hydrous glass was ground to grain sizes of <20 μm and used as starting material for the isotope exchange and crystallisation experiments. For this study eight batches of ''isotopically normal'' hydrous glass were synthesised, each analysed by electron microprobe (Table EA-2). The difference to 100% in the electron microprobe analysis was interpreted as the amount of H_2O dissolved in the glasses (e.g., Devine et al., 1995; Morgan and London, 1996; Berndt et al., 2005). In addition, the H_2O concentrations of selected glasses were determined by Karl-Fischer titration (KFT) (Behrens and Stuke, 2003; Leschik et al., 2004). Although, the ''by-difference-method'' for water determination using the EMPA has a relatively high uncertainty of at least ± 0.5 wt%, the results of both methods are in very good agreement (Table EA-2), with exception of NSLsyn01. The EMPA measurements show homogeneous distribution of water in the glasses.

2.1.3. ^{57}Fe enriched glasses

For the kinetic tracer experiments we doped the NSLsyn glass with a ^{57}Fe isotope tracer. For this study two batches of hydrous ^{57}Fe-enriched NSLsyn glass were synthesised

(Table EA-2, $NSLsyn04_{spike}$ and $NSLsyn06_{spike}$). Electron microprobe transects were measured on three glass pieces of each charge to ensure compositional homogeneity. Fe isotope analyses were performed on two different glass pieces of each batch (Table 1). FeO_{total} concentration of the ^{57}Fe-enriched glasses are slightly lower (~0.3–0.7 wt% FeO_{total} less) than those of "unspiked" hydrous glasses (Table EA-2). Probably small amounts of iron were lost to the capsule during the initial melting under dry conditions in the internally heated pressure vessel (IHPV) (Berndt et al., 2005). No iron loss was observed after synthesis of water-bearing glasses.

2.2. Experimental design

2.2.1. Kinetic tracer experiments

The kinetics of iron isotope exchange between pyrrhotite and silicate melt were determined using the ^{57}Fe enriched glass and natural pyrrhotite with "natural" ^{57}Fe abundance. The use of enriched isotope tracers to evaluate the kinetics of isotope exchange has a long history (Mills and Urey, 1940) and was already successfully applied to the iron isotopic system by Johnson et al. (2002). The initial difference in $^{57}Fe/^{54}Fe$ between pyrrhotite ($^{57}Fe/^{54}Fe$ ~0.363) and melt ($NSLsyn04_{spike}$: $^{57}Fe/^{54}Fe$ ~ 0.951) is much larger than any kinetic or equilibrium isotope fractionation in nature. The high analytical precision allows an accurate assessment of the kinetics of iron isotope exchange and the timescale required to attain isotopic equilibrium at the given *P–T*-conditions. For each experiment approximately 80 mg of ^{57}Fe enriched hydrous glass powder ($NSLsyn04_{spike}$, Table 1) was mixed with ~5 mg of natural pyrrhotite powder (sample K, Table 1) and sealed in a gold capsule. Experiments were performed in the IHPV at 900 °C and 500 MPa for 2 h, 24 h, 48 h and 120 h, respectively, to obtain a time-resolved approach to isotopic equilibrium.

2.2.2. Isotope exchange experiments

For each of the investigated temperatures four or five capsules were prepared containing ~80 mg of hydrous NSLsyn glass powder (~4 wt% H_2O) mixed with ~5 mg of natural pyrrhotite powder. Four different natural pyrrhotites (Table 1) were used to vary the initial differences in iron isotope composition between pyrrhotite and glass. All capsules of each set were processed simultaneously in the IHPV at 500 MPa and either 840, 900 or 1000 °C, to ensure identical experimental conditions. Each experimental set also included at least one capsule with ^{57}Fe enriched glass powder mixed with pyrrhotite to assess the extent of equilibration for the given experimental conditions.

2.2.3. Crystallisation experiments

Hydrous NSLsyn glass powder (~4 wt% H_2O, Table EA-2) was mixed with various amounts of elemental sulphur (ChemPur®, 99.99% purity) and sealed in Au capsules to crystallise pyrrhotite. Preliminary tests with relatively large amounts of sulphur (up to ~14 wt% S in the capsule) resulted in the formation of large Fe–S-rich fluid bubbles and an inhomogeneous Fe distribution in the melt (Fig. 1A). By reducing the concentration of elemental sulphur to <0.53 wt%, pyrrhotite was crystallised with a coexisting homogeneous melt free of large Fe–S-rich fluid bubbles. Small vesicles (<1 μm) were occasionally present, probably due to trapped nitrogen during capsule preparation.

Three or four capsules with different initial Fe:S ratios (ranging from about 6:1 to 12:1) were processed simultaneously in the IHPV at 500 MPa and at a temperature of 840, 900 or 1000 °C. Pyrrhotite crystallised preferentially along the former grain boundaries of the glass powder (Fig. 1B) and was often accumulated in a few, large clusters probably due to initial inhomogeneous distribution of S in the loaded charge. To improve homogenous distribution of pyrrhotite in the samples, the experiments were interrupted after 24 h. Samples were reground, sealed again in new Au capsules and processed in the IHPV for another five to six days at identical experimental conditions. One capsule was added to each run that only contained hydrous glass powder. The redox state of iron in those samples was determined by wet chemistry using a colorimetric method (Wilson, 1960).

2.2.4. Run conditions

During the experiments in the IHPV temperature was measured next to the capsules (typically capsules had an inner diameter of 4 mm, a wall thickness of 0.2 mm, and a length of ~15 mm) using three K-type thermocouples with an accuracy of better than ±7 °C (A. Meisen, personal communication). The temperature variation across the capsule assemblage was <5 °C and temperature stability was always better than ±2 °C. Pressure was measured with an uncertainty of about 1 MPa and the stability was within 5 MPa. Heating to the desired run temperature was done isobarically at 500 MPa at a rate of 30 °C/min. Oxygen fugacity is imposed by the intrinsic hydrogen fugacity of the IHPV. At water-saturated conditions in the capsule the oxygen fugacity is close to that of the $MnO–Mn_3O_4$ buffer ($\log fO_2 \sim NNO+3.5$; see Berndt et al. (2002)). In all experiments the melts were H_2O undersaturated and, hence, the prevailing oxygen fugacity in the capsule was lower than NNO+3.5. For peralkaline rhyolite the relationship between water solubility in the melt and water activity is not known. To estimate the oxygen fugacity we assumed for simplicity that the water activity aH_2O is proportional to the water concentration in the melt. At 4 wt% H_2O dissolved in the melt and 500 MPa, this approach probably slightly overestimates the water activity (see Fig. 4 of Tamic et al. (2001) for the variation of water solubility in rhyolitic melts as a function of the mole fraction of water in the fluid), but aH_2O is estimated to be accurate within a factor of two. Using a water solubility of 10.93 wt% determined for peralkaline rhyolite (NSL) at 800 °C and 500 MPa (Behrens and Jantos, 2001), the esti-

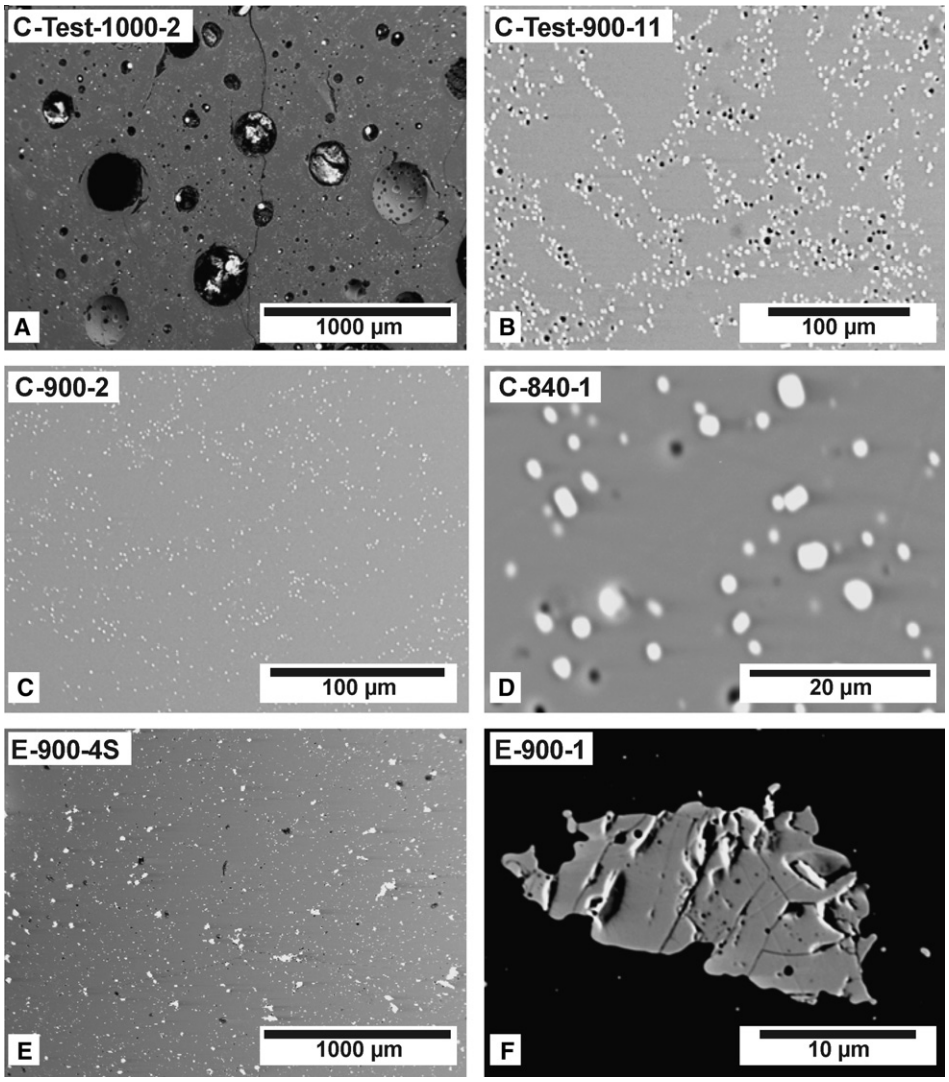

Fig. 1. Back scattered electron images of representative experimental run products. (A) Preliminary crystallisation experiments (1000 °C, 500 MPa, 24 h) with high amounts of sulphur (14.16 wt% S) resulted in formation of large Fe–S-rich fluid bubbles. (B) Short term crystallisation experiments (900 °C, 500 MPa, 24 h, 0.29 wt% S added) show preferential pyrrhotite (light colour) formation along the former grain boundaries of the glass powder. (C and D) Typical images of run products from re-homogenised crystallisation experiments with initial S contents <0.54 wt%. (E) Representative image of run products from exchange experiments. A pyrrhotite crystal is shown in detail in (F). The crystal shows a dissolution texture, but a subhedral crystal shape is still preserved.

mated log fO_2 is NNO+2.6. According to Gaillard et al. (2002) redox equilibrium is attained after ~3 h under our experimental conditions.

After the run the samples were isobarically quenched to room temperature at an initial cooling rate of ~200 °C/min by turning off the power of the furnace. The capsules were weighed before and after the IHPV runs to ensure that they remained closed during the experiments.

2.2.5. Characterisation of run products

Thin sections of all run products, except for samples E-840-5S and C-840-3, were prepared for microprobe analysis. The remaining sample was ground in an agate mortar to grain sizes of <5 µm for Fe isotope analysis. Selected samples were examined by XRD for phase identification. All microprobe analyses of pyrrhotites and glasses were done on a Cameca SX-100 (see Electronic annex for details on analytical conditions). Water concentrations in the glasses were estimated from electron microprobe analysis using the ''by-difference-method''.

2.3. Isotope analysis

2.3.1. Phase separation

The run products of all experiments, pyrrhotite and silicate glass, need to be separated before chemical Fe purification and subsequent isotope analysis using solution multi collector inductively coupled plasma mass spectrometry (MC-ICP-MS). In most experiments, in particular in the crystallisation experiments, grain sizes of pyrrhotite were too small for physical separation by para-magnetism or heavy liquids. Therefore, pyrrhotite was selectively re-

moved from the glass by dissolution in hydrochloric acid. However, no complete phase separation could be attained with this method. This leads to a systematic underestimate of the measured fractionation factors. Therefore, a correction for this cross-contamination during phase separation was applied to the measured Fe isotope data of pyrrhotite and glass (see Electronic annex for details on the phase separation and the corrections). The extent of the corrections can be seen in Tables 2 and 3.

Iron was separated from other elements by anion-exchange chromatography as described in Schoenberg and von Blanckenburg (2005). Before and after column chemistry, Fe concentrations were measured by ICP-OES to ensure quantitative elution of Fe from the anion exchange resin (DOWEX AG© 1×8 100–200 mesh) and to verify that matrix elements were removed efficiently. Total procedural Fe blanks were always below 60 ng. This is more than four orders of magnitude less than Fe processed and is considered negligible.

2.3.2. Mass spectrometry and data presentation

All iron isotope measurements were carried out on a ThermoFinnigan Neptune MC-ICP-MS using the analytical protocol described by Schoenberg and von Blanckenburg (2005). The standard-sample bracketing technique was used to correct for instrumental mass bias and the commercially available iron standard IRMM-014 was used as bracketing reference standard. Iron isotope data are reported in the δ-notation, which gives the permil deviation of the $^{56}Fe/^{54}Fe$ or $^{57}Fe/^{54}Fe$ ratio of the sample relative to that of the IRMM-014 standard, e.g.:

$$\delta^{56}Fe_{sample} = \left[\left(\frac{^{56}Fe}{^{54}Fe}sample \Big/ \frac{^{56}Fe}{^{54}Fe}IRMM\text{-}014\right) - 1\right] \cdot 1000 \quad [‰]. \tag{1}$$

The long-term external reproducibility for Fe isotope measurements, determined by replicate analysis of standards and samples of different matrices, is $\pm 0.049‰$ and $\pm 0.071‰$ (2 standard deviation, 2σ) for $\delta^{56}Fe$ and $\delta^{57}Fe$, respectively (Schoenberg and von Blanckenburg, 2005). We routinely analysed our internal laboratory standard JM (commercially available pure Fe wire) within each analytical session to assess the accuracy of the measurements. During the course of this study the measured Fe isotope composition of the JM standard was $\delta^{56}Fe = 0.422 \pm 0.043‰$ and $\delta^{57}Fe = 0.631 \pm 0.072‰$ (2σ, $n = 64$), which is in excellent agreement with previous measurements ($\delta^{56}Fe = 0.423 \pm 0.046‰$ and $\delta^{57}Fe = 0.624 \pm 0.073‰$) given by Schoenberg and von Blanckenburg (2005). Measured Fe isotope differences between pyrrhotite (p) and glass (g) are expressed by the fractionation factor α

$$\alpha_{p-g} = \frac{1000 + \delta^{56}Fe_p}{1000 + \delta^{56}Fe_g} \tag{2}$$

or by the approximation

$$\Delta^{56}Fe_{p-g} = \delta^{56}Fe_p - \delta^{56}Fe_g \approx 10^3 \ln \alpha_{p-g} \tag{3}$$

3. Results

All experiments contained pyrrhotite and glass as the only reaction products (Fig. 1), except for samples E-900-1, E-840-2 and E840-5S, where small amounts of additional quartz with crystal sizes <10 μm were present. However, quartz is not expected to affect Fe isotope partitioning between pyrrhotite and silicate melt. In the crystallisation experiments small pyrrhotite crystals (<1 μm) were homogeneously distributed in the run products. Pyrrhotite crystal contents in these experiments, estimated by mass balance of iron, were below 1.5 wt%. EMPA transects through the samples revealed homogeneous melt compositions and H_2O concentrations identical with those of the starting materials within analytical uncertainty (Table EA-2).

The redox state of Fe, expressed as $Fe^{2+}/\Sigma Fe$ ratio, in the pure hydrous rhyolitic melt (measured by wet-chemistry) does not vary significantly with temperature (0.37 ± 0.01 (1σ, $n = 3$) at 840 °C, 0.39 ± 0.01 (1σ, $n = 5$) at 900 °C and 0.37 ± 0.02 (1σ, $n = 7$) at 1000 °C). The temperature independence of the $Fe^{2+}/\Sigma Fe$ ratio (average: 0.38 ± 0.02, 1σ, $n = 15$) is consistent with experimental findings of Gaillard et al. (2001).

In the crystallisation experiments pyrrhotite crystallisation lowered the FeO_{total} in the glasses by 0.02–0.79 wt% compared to the starting material. On the other hand, in exchange experiments FeO_{total} slightly increased, because the added pyrrhotite was partially dissolved to saturate the melt with sulphur (Fig. 2 and Table EA-5). The differences in the sulphur contents of the post-experimental glasses can be explained by variations in iron content of the melt and in temperature (Botcharnikov et al., 2004).

Only hexagonal pyrrhotite was found by XRD in run products of crystallisation and exchange experiments. The monoclinic pyrrhotites MV and R, used as starting material in several experiments (Table 2) changed to hexagonal crystal structure, as expected for high-temperature pyrrhotites (Vaughan and Craig, 1978). Compositions of pyrrhotites after the exchange experiments are given in Table EA-5. Since the crystal size of pyrrhotites from the crystallisation experiments were <1 μm it was not possible to analyse them by EMPA.

3.1. Isotope exchange kinetics

The kinetics of Fe isotope exchange and the time scale to attain isotopic equilibrium in the system was investigated in detail at 900 °C and 500 MPa using ^{57}Fe enriched glass. Fig. 3 shows that the $\delta^{57}Fe$ of the melt decreased rapidly with experimental runtime through isotope exchange with the coexisting pyrrhotite, which correspondingly increased in $\delta^{57}Fe$. A close approach to Fe isotope equilibrium

Table 2
Summary of exchange and kinetic tracer experiments

Experiment	Starting materials[a]	Phase[b]	Replicate analyses		Averages—measured[c]		Averages—corrected[d]				$\Delta^{56}Fe_{initial}$[e]	$\Delta^{56}Fe_{final}$[e]	$\Delta^{56}Fe_{final\text{-}initial}$[e]	$\Delta^{56}Fe_{pyrrhotite\text{-}melt}$[f]	Fractional approach to equilibrium[g]			
			$\delta^{56}Fe$	$\delta^{57}Fe$	$\delta^{56}Fe$	$\delta^{57}Fe$	$\delta^{56}Fe$	2σ	$\delta^{57}Fe$	2σ					F(N & C)	$F(\Delta)$	$F(\delta)_p$	$F(\delta)_g$
Exchange experiments																		
840 °C, 144 h experimental runtime																		
E-840-1	NSLsyn12	g	−0.549	−0.790	−0.549	−0.790	−0.41	0.12	−0.57	0.19	−0.80 ± 0.07	−0.50 ± 0.13	0.30 ± 0.15	−0.37 ± 0.24	0.72			
	+ B	p	−0.908	−1.349	−0.908	−1.349												
E-840-2	NSLsyn12	g	−0.238	−0.355	−0.238	−0.355	−0.17	0.07	−0.26	0.10	−0.12 ± 0.07	−0.23 ± 0.09	−0.11 ± 0.11					
	+ K	p	−0.407	−0.599	−0.407	−0.599												
E-840-3	NSLsyn12	g	−0.317	−0.471	−0.317	−0.471	−0.15	0.14	−0.23	0.20	−0.80 ± 0.07	−0.60 ± 0.15	0.20 ± 0.17					
	+ R	p	−0.751	−1.080	−0.751	−1.080												
E-840-4S	$NSLsyn06_{spike}$	g	−0.035	230.525	−0.025	230.544	0.11	0.12	243.49	10.2	−0.36 ± 0.07	−0.47 ± 0.13	−0.11 ± 0.14			0.89	0.98	0.82
	+ K	g	−0.016	230.563														
		p	−0.391	197.218	−0.367	197.262												
		p	−0.343	197.306														
E-840-5S	$NSLsyn06_{spike}$	g	−0.382	209.934	−0.372	209.982	−0.24	0.11	219.31	7.3	−1.04 ± 0.07	−0.46 ± 0.12	0.58 ± 0.14			0.92	0.94	0.91
	+ B	g	−0.361	210.030														
		p	−0.719	185.968	−0.706	186.002												
		p	−0.693	186.037														
900 °C, 120 h experimental runtime																		
E-900-1	NSLsyn09	g	−0.613	−0.854	−0.613	−0.854	−0.49	0.11	−0.64	0.18	−0.80 ± 0.07	−0.44 ± 0.12	0.36 ± 0.14	−0.35 ± 0.10	0.86			
	+ B	p	−0.930	−1.399	−0.930	−1.399												
E-900-2	NSLsyn09	g	−0.339	−0.542	−0.339	−0.542	−0.21	0.11	−0.37	0.15	−0.47 ± 0.07	−0.46 ± 0.12	0.02 ± 0.14					
	+ R	p	−0.668	−0.980	−0.668	−0.980												
E-900-3	NSLsyn09	g	−0.292	−0.393	−0.292	−0.393	−0.22	0.08	−0.26	0.12	−0.12 ± 0.07	−0.26 ± 0.09	−0.14 ± 0.11					
	+ K	p	−0.482	−0.723	−0.482	−0.723												
E-900-4S	$NSLsyn04_{spike}$	g	0.190	713.539	0.179	713.462	0.29	0.10	728.31	11.7	−1.09 ± 0.07	−0.40 ± 0.11	0.69 ± 0.13			0.97	0.96	0.97
	+ K	g	0.169	713.386														
		p	−0.108	675.286	−0.110	675.289												
		p	−0.111	675.293														
1000 °C, 120 h experimental runtime																		
E-1000-1	NSLsyn11	g	−0.635	−0.910	−0.635	−0.910	−0.48	0.13	−0.67	0.20	−0.80 ± 0.07	−0.57 ± 0.14	0.23 ± 0.16	−0.44 ± 0.10	0.93			
	+ B	p	−1.045	−1.537	−1.045	−1.537												
E-1000-2	NSLsyn09	g	−0.402	−0.557	−0.402	−0.557	−0.27	0.11	−0.38	0.16	−0.47 ± 0.07	−0.46 ± 0.12	0.02 ± 0.14					
	+ R	p	−0.735	−1.043	−0.731	−1.023												
		p	−0.727	−1.002														
E-1000-3S	$NSLsyn06_{spike}$	g	−0.154	206.409	−0.144	206.446	−0.03	0.10	206.72	0.23	−0.36 ± 0.07	−0.40 ± 0.11	−0.04 ± 0.13			1.00	1.02	0.98
	+ K	g	−0.133	206.482														
		p	−0.416	205.776	−0.430	205.736												
		p	−0.443	205.695														
E-1000-4S	$NSLsyn06_{spike}$	g	−0.435	237.067	−0.430	237.068	−0.31	0.11	238.11	0.83	−1.04 ± 0.07	−0.44 ± 0.12	0.60 ± 0.14			0.99	0.98	1.01
	+ B	g	−0.425	237.069														
		p	−0.725	234.384	−0.746	234.377												
		p	−0.766	234.369														

(*continued on next page*)

Table 2 (*continued*)

Experiment	Starting materials[a]	Phase[b]	Replicate analyses		Averages—measured[c]		Averages—corrected[d]				$\Delta^{56}Fe_{initial}$[e]	$\Delta^{56}Fe_{final}$[e]	$\Delta^{56}Fe_{final\text{-}initial}$[e]	$\Delta^{56}Fe_{pyrrhotite\text{-}melt}$[f]	Fractional approach to equilibrium[g]		
			δ^{56}Fe	δ^{57}Fe	δ^{56}Fe	δ^{57}Fe	δ^{56}Fe	2σ	δ^{57}Fe	2σ					F(N & C)	$F(\Delta)$	$F(\delta)_p$ $F(\delta)_g$
Kinetic tracer experiments																	
900 °C, experiment runtimes varied																	
E-900-1S	NSLsyn04$_{spike}$	g	0.259	903.693	0.239	903.602	0.40	0.14	1104.06	157.7					0.56	0.57	0.55
(2 h)	+ K	g	0.218	903.512													
		p	−0.197	388.135	−0.184	388.135											
		p	−0.171	388.135													
E-900-2S	NSLsyn04$_{spike}$	g	0.296	726.949	0.296	726.949	0.45	0.13	774.20	37.2					0.90	0.90	0.89
(24 h)	+ K	p	−0.110	605.452	−0.110	605.452											
E-900-3S	NSLsyn04$_{spike}$	g	0.186	689.599	0.186	689.599	0.32	0.11	715.54	20.4					0.94	0.92	0.96
(48 h)	+ K	p	−0.150	622.892	−0.150	622.892											

All experiments were performed at 500 MPa.

[a] Mixtures of hydrous glass (~4 wt% H_2O) and pyrrhotite powder (see Tables 1 and EA-2). Numbers refer to the different synthesised NSLsyn glass batches. Suffix spike denotes ^{57}Fe enriched glass.

[b] Separated glass (g) or pyrrhotite (p) fraction.

[c] Analytical uncertainty (long-term external reproducibility (2σ)) for "unspiked" samples on the Neptune mass spectrometer with standard-sample bracketing is ±0.049‰ on δ^{56}Fe and ±0.071‰ on δ^{57}Fe.

[d] Measured values of the separated glass fractions were corrected for uncomplete separation from pyrrhotite (see Electronic annex for details).

[e] Uncertainties for Δ^{56}Fe values are calculated by error propagation of the uncertainties in δ^{56}Fe values of the involved phases, including errors associated with corrections, if applied.

[f] Fractionation factor according to the method of Northrop and Clayton (1966). Given uncertainty is the error on the y-intercept derived from the error weighted linear regression.

[g] $F(\delta)$p and $F(\delta)$g values were calculated according to Eq. (4), where p and g refer to the pyrrhotite or the glass fraction, respectively. $F(\Delta)$ values are calculated using Eq. (5). F(N & C) values were derived from Fig. 4, where $F = (-1/\text{slope})$.

(>90%) between these two phases is already attained after 24 h.

The extent of isotope equilibration $F(\delta)$ at a given runtime can be described for each phase by

$$F(\delta) = \frac{\delta^{57}Fe_{final} - \delta^{57}Fe_{initial}}{\delta^{57}Fe_{equilibrium} - \delta^{57}Fe_{initial}} \quad (4)$$

where $\delta^{57}Fe_{initial}$ and $\delta^{57}Fe_{final}$ denote the Fe isotope composition of this phase before and after the experiment (e.g., Criss et al., 1987; Johnson et al., 2004). $\delta^{57}Fe_{equilibrium}$ is the equilibrium isotope composition of this phase, which is identical to the bulk Fe isotope composition of the mixture in the capsule if full equilibration is reached. This presumption is valid because any equilibrium Fe isotope fractionation between melt and pyrrhotite is insignificant compared to the difference in δ^{57}Fe between the two phases even at $F = 0.99$. The bulk Fe isotope composition can be calculated from the respective amounts of iron and corresponding $\delta^{57}Fe_{initial}$ values of the starting materials. Alternatively, F can also be expressed in terms of Δ^{57}Fe:

$$F(\Delta) = \frac{\Delta^{57}Fe_{final} - \Delta^{57}Fe_{initial}}{\Delta^{57}Fe_{equilibrium} - \Delta^{57}Fe_{initial}} \quad (5)$$

Both expressions (Eqs. (4) and (5)) were used to evaluate the fractional approach to equilibrium.

The atomic processes which control the isotope exchange kinetics in our experiments are not fully clear. However, isotope exchange kinetics observed in other experimental systems (e.g., Cole and Chakraborty, 2001) often follow the general form shown in Fig. 3, which is rapid initial exchange followed by slower exchange. Since small amounts of pyrrhotite are dissolved in the initial stages of the experiments, it is possible that the isotope exchange reaction is dominated by dissolution and recrystallisation in the early stages, as indicated by more than 50% exchange after the 2 h experiment. Recrystallisation of pyrrhotite is also supported by XRD measurements on the run products, demonstrating a change from initially monoclinic to hexagonal symmetry. After 24 h the approach to the equilibrium value slows (Fig. 3). This might be due to a diffusion-controlled exchange mechanism, governed by the diffusivity of Fe in pyrrhotite and in the melt. However, the experiments demonstrate that a very close approach to equilibrium is already reached after 48 h.

3.2. Isotope exchange experiments

The method of Northrop and Clayton (1966), originally developed to determine oxygen and carbon isotope equilibrium fractionation factors, was applied to determine Fe equilibrium isotope fractionation factors between pyrrhotite and silicate melt at high temperatures. This method allows the determination of an equilibrium fractionation factor between two phases at given conditions from a set of partial exchange experiments. Partial isotope exchange

Table 3
Summary of crystallisation experiments

Experiment	Starting glass	Fe:$S_{initial}$[a]	$S_{initial}$ (wt%)[a]	Phase[b]	Replicate analyses		Averages—measured[d]		Averages—corrected[e]				$\Delta^{56}Fe_{pyrrhotite\text{-}melt}$[f]	Averages	$fFe_{transfer}$[h]
					$\delta^{56}Fe$	$\delta^{57}Fe$	$\delta^{56}Fe$	$\delta^{57}Fe$	$\delta^{56}Fe$	2σ	$\delta^{57}Fe$	2σ		$\Delta^{56}Fe_{pyrrhotite\text{-}melt}$[g]	
840 °C, experimental runtime 24 + 144 h[c]															
C-840-1	NSLsyn08	9.1:1	0.36	g	−0.131	−0.213	−0.122	−0.193					−0.33 ± 0.07	−0.35 ± 0.10	0.189 ± 0.098
				g	−0.113	−0.172									
				p	−0.427	−0.604	−0.438	−0.608	−0.46	0.05	−0.63	0.07			
				p	−0.449	−0.613									
C-840-2	NSLsyn08	8.8:1	0.37	g	−0.100	−0.219	−0.126	−0.192					−0.31 ± 0.08		0.101 ± 0.101
				g	−0.152	−0.165									
				p	−0.416	−0.600	−0.404	−0.599	−0.44	0.06	−0.65	0.09			
				p	−0.392	−0.598									
C-840-3	NSLsyn08	8.5:1	0.40	g	−0.265	−0.354	−0.244	−0.349					−0.40 ± 0.07		~0.145[i]
				g	−0.223	−0.343									
				p	−0.624	−0.948	−0.618	−0.933	−0.65[i]	0.05	−0.98[i]	0.08			
				p	−0.611	−0.918									
900 °C, experimental runtime 24 + 120 h[c]															
C-900-1	NSLsyn05	8.8:1	0.37	g	−0.207	−0.301	−0.198	−0.311					−0.41 ± 0.09	−0.38 ± 0.10	0.092 ± 0.078
				g	−0.190	−0.321									
				p	−0.550	−0.800	−0.558	−0.821	−0.60	0.07	−0.89	0.10			
				p	−0.565	−0.841									
C-900-2	NSLsyn07	6.2:1	0.54	g	−0.217	−0.349	−0.217	−0.349					−0.37 ± 0.07		0.168 ± 0.049
				p	−0.575	−0.815	−0.561	−0.808	−0.58	0.05	−0.84	0.07			
				p	−0.547	−0.801									
C-900-3	NSLsyn07	12.2:1	0.27	g	−0.212	−0.362	−0.220	−0.344					−0.32 ± 0.07		0.098 ± 0.039
				g	−0.229	−0.326									
				p	−0.511	−0.735	−0.502	−0.723	−0.54	0.05	−0.77	0.07			
				p	−0.492	−0.710									
C-900-4	NSLsyn07	8.4:1	0.40	g	−0.240	−0.372	−0.246	−0.374					−0.43 ± 0.09		0.069 ± 0.042
				g	−0.252	−0.376									
				p	−0.599	−0.871	−0.608	−0.877	−0.67	0.07	−0.97	0.10			
				p	−0.616	−0.883									

(*continued on next page*)

Table 3 (*continued*)

Experiment	Starting glass	Fe:$S_{initial}$ [a]	$S_{initial}$ (wt%) [a]	Phase [b]	Replicate analyses		Averages—measured [d]		Averages—corrected [e]				$\Delta^{56}Fe_{pyrrhotite\text{-}melt}$ [f]	Averages	$fFe_{transfer}$ [h]
					$\delta^{56}Fe$	$\delta^{57}Fe$	$\delta^{56}Fe$	$\delta^{57}Fe$	$\delta^{56}Fe$	2σ	$\delta^{57}Fe$	2σ		$\Delta^{56}Fe_{pyrrhotite\text{-}melt}$ [g]	
1000 °C, experimental runtime 24 + 120 h [c]															
C-1000-1	NSLsyn10	8.8:1	0.37	g	−0.149	−0.215	−0.145	−0.239					−0.37 ± 0.39	−0.30 ± 0.23	0.005 ± 0.052
				g	−0.141	−0.262									
				p	−0.255	−0.362	−0.244	−0.328	−0.52	0.39	−0.57	0.35			
				p	−0.232	−0.293									
C-1000-2	NSLsyn07	6.0:1	0.53	g	−0.059	−0.086	−0.065	−0.088					−0.16 ± 0.09		0.041 ± 0.037
				g	−0.072	−0.089									
				p	−0.185	−0.266	−0.191	−0.267	−0.23	0.08	−0.32	0.12			
				p	−0.197	−0.268									
C-1000-3	NSLsyn07	11.1:1	0.30	g	−0.170	−0.298	−0.162	−0.274					−0.35 ± 0.36		0.004 ± 0.047
				g	−0.155	−0.250									
				p	−0.236	−0.349	−0.236	−0.349	−0.51	0.36	−0.63	0.37			

All experiments were performed at 500 MPa.

[a] Iron to sulphur weight ratio. The variation in this ratio was obtained by varying the amount of S added to the capsules.

[b] Separated glass (g) or pyrrhotite (p) fraction.

[c] Runs were interrupted after one day to rehomogenise the charge.

[d] Analytical uncertainty (long-term external reproducibility (2σ)) on the Neptune mass spectrometer with standard-sample bracketing is ±0.049‰ on $\delta^{56}Fe$ and ±0.071‰ on $\delta^{57}Fe$.

[e] Measured values of the separated pyrrhotite fractions were corrected for contamination with Fe from glass during phase separation (see Electronic annex for details).

[f] The given error results from propagation of the uncertainties in $\delta^{56}Fe$ values of the involved phases.

[g] The given error is the two standard deviation (2σ) of all $\Delta^{56}Fe_{pyrrhotite\text{-}melt}$ values obtained at a certain temperature.

[h] Fraction of Fe transferred from the melt to pyrrhotite during the crystallisation experiments, calculated from measured FeO contents (H_2O free normative concentrations; Tables EA-2 and EA-5) in the glass before and after the experiments: $fFe_{transfer} = (cFeO_{start\ glass} - cFeO_{after\ exp})/cFeO_{start\ glass}$. Given uncertainties result from propagation of analytical errors of FeO concentrations (EMPA).

[i] $fFe_{transfer}$ for C-840-2 was estimated on the basis of experiments C-840-1 and C-840-3, because no thin section for electron microprobe analysis was prepared from this sample. Therefore, correction on the $\delta^{56}Fe$ of pyrrhotite is also based on this estimate.

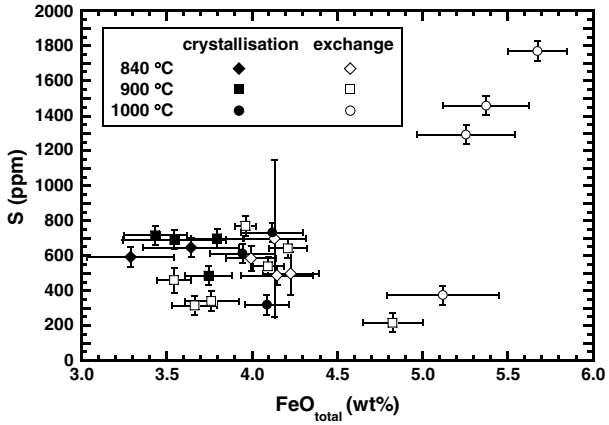

Fig. 2. Sulphur contents in the post-experimental glasses of crystallisation and isotope exchange experiments as a function of FeO_{total}.

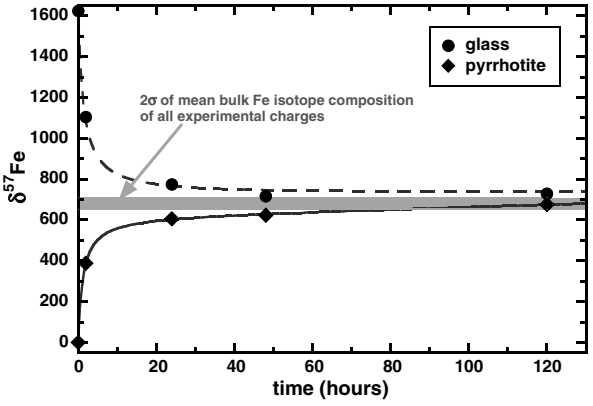

Fig. 3. Kinetics of iron isotope exchange between pyrrhotite and ^{57}Fe-enriched silicate melt at 900 °C and 500 MPa. A close approach to isotopic equilibrium (grey shaded band) is already attained after 24 h. The solid trend line was fitted to the pyrrhotite data. This in turn was used to compute the corresponding dashed line for the glass fraction to satisfy mass balance. The grey area represents the variation in the bulk Fe isotope composition of all experimental charges (average $\delta^{57}Fe = 682 \pm 29‰$ (2σ)). Each capsule was filled with an individually prepared mixture of pyrrhotite and glass powder.

reactions can be described mathematically by the following equation (Northrop and Clayton, 1966):

$$\ln \alpha_{initial} = \ln \alpha_{equilibrium} - 1/F \cdot (\ln \alpha_{final} - \ln \alpha_{initial}) \quad (6)$$

where $\alpha_{initial}$ and α_{final} represent the differences in isotope composition between the two phases of interest at the beginning and at the end of the experiment, respectively, expressed as fractionation factor (see Eq. (2)). $\alpha_{equilibrium}$ is the difference in isotope composition between the two phases when equilibrium is reached, and F is the degree of equilibration of the system (see Eqs. (4) and (5)) after a certain experimental runtime.

The equilibrium fractionation factor can be derived from the y-intercept of a plot of $\ln\alpha_{initial}$ versus $\ln\alpha_{final} - \ln\alpha_{initial}$ data. Alternatively, if α values are close to unity, as in our study, plots of $\Delta^{56}Fe_{inital}$ vs. ($\Delta^{56}Fe_{final} - \Delta^{56}Fe_{initial}$) are equivalent (see Fig. 4).

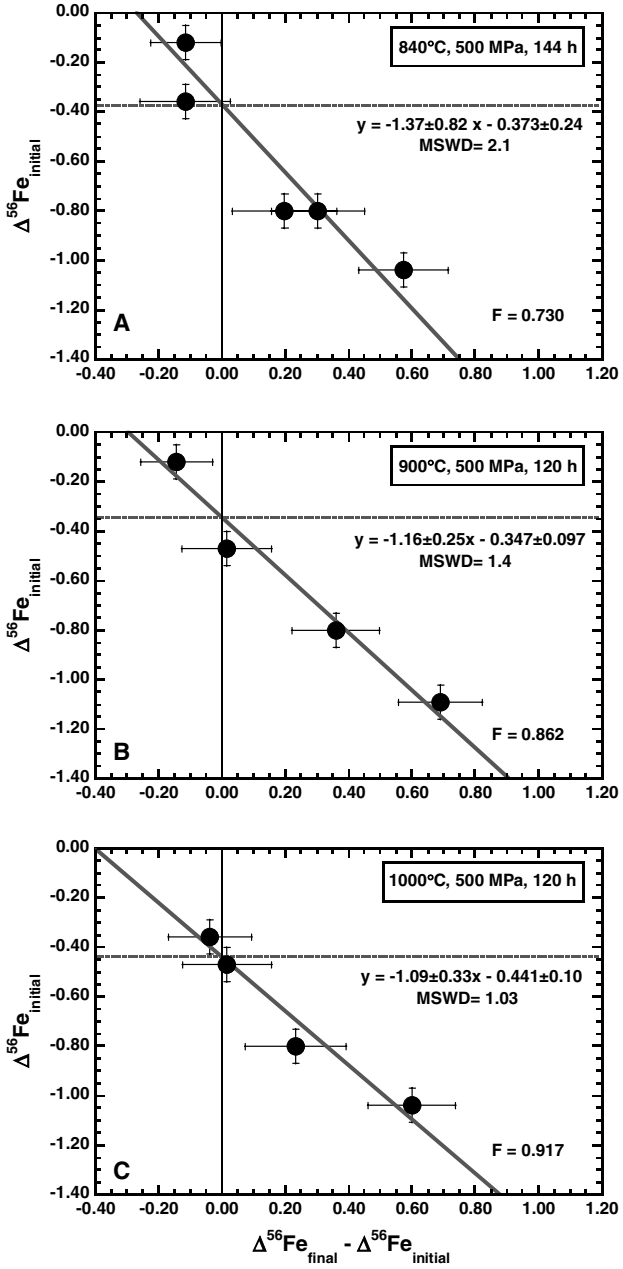

Fig. 4. Iron isotope exchange between pyrrhotite and silicate melt at temperatures of (A) 840 °C, (B) 900 °C and (C) 1000 °C presented according to Northrop and Clayton (1966). $\Delta^{56}Fe_{initial}$ and $\Delta^{56}Fe_{final}$ represent the differences in Fe isotope composition between pyrrhotite and glass at the start and at the end of each experiment (Table 2). The y-intercept of the liner regression corresponds to the equilibrium isotope fractionation factor and F (=−1/slope) to the extent of equilibration.

The equilibrium fractionation factor between pyrrhotite and silicate melt at each experimental temperature was determined by a least-squares fit accounting for individual errors using the method of York (1969) as implemented in *Isoplot* (Ludwig, 2001). The linearity of the data (Fig. 4) indicates that boundary conditions for application of the partial-exchange method are satisfied. Criss (1999) proposed an iterative approach for solving Eq. (6). We applied

both methods to our data and obtained identical results. For simplicity, we implemented the conventional method of Northrop and Clayton (1966).

The fractional approach to equilibrium, determined from the slopes in Fig. 4 ($F = -1/\text{slope}$) was 0.72 at 840 °C (6 days), 0.86 at 900 °C (5 days) and 0.93 at 1000 °C (5 days) (denoted as F(N & C) in Table 2). These values are generally lower than $F(\delta)_p$ values calculated by Eq. (4) from the ^{57}Fe-enriched samples included in each experimental serie. However, these discrepancies lie within the uncertainties of the slopes derived by linear regression. It must be noted that the slopes in Fig. 4 are associated with relatively high uncertainties (Fig. 4), but the y-intercepts, which are the quantitatively relevant values here, are more precise. The derived fractionation factors expressed as $\Delta^{56}Fe_{pyrrhotite\text{-}melt}$ are $-0.37 \pm 0.24‰$ at 840 °C, $-0.35 \pm 0.10‰$ at 900 °C and $-0.44 \pm 0.10‰$ at 1000 °C (Table 2). The negative sign of the fractionation factor indicates that pyrrhotite preferentially incorporates lighter Fe isotopes relative to the coexisting silicate melt.

3.3. Crystallisation experiments

The crystallisation experiments corroborate the result of the exchange experiments in that Fe in pyrrhotite is isotopically lighter than in the silicate melt. The measured $\Delta^{56}Fe_{pyrrhotite\text{-}melt}$ values of different samples, run at the same temperature, show good internal consistency, independent from the initial sulphur content (Table 3). Average $\Delta^{56}Fe_{pyrrhotite\text{-}melt}$ values are $-0.35 \pm 0.10‰$ at 840 °C, $-0.38 \pm 0.10‰$ at 900 °C and $-0.30 \pm 0.23‰$ at 1000 °C (Table 3). Pyrrhotite crystal content varied in the experimental products and was quantified by comparing the iron concentration of the starting glass and the post-experimental glass. Since pyrrhotite is the only Fe-bearing crystalline phase, the fraction of Fe transferred from the melt to pyrrhotite, $f\text{Fe}_{transfer}$ can be calculated as $(c\text{FeO}_{start\ glass} - c\text{FeO}_{glass\ after\ exp})/c\text{FeO}_{start\ glass}$. In the calculation we used H_2O-free normative FeO concentrations derived from the analyses listed in Tables EA-2 and EA-5. The obtained values of $f\text{Fe}_{transfer}$ range from 0.004 to 0.189 (Table 3). However, it must be noted that these calculations have high uncertainties due to the low-pyrrhotite contents and hence small changes in the Fe concentration in the melt, which are hardly detectable within analytical precision. This is also reflected in the large errors assigned to the corrected δ^{56}Fe values of pyrrhotite of two of the 1000 °C experiments, which have very low pyrrhotite contents (Table 3).

Fig. 5 shows the measured Fe isotope compositions of corresponding pyrrhotite–glass pairs in comparison with the theoretical mass balance lines for equilibrium Fe isotope fractionation in a closed system. Except for one 1000 °C experiment (C-1000-2), there is good agreement between measured and predicted Fe isotope distributions.

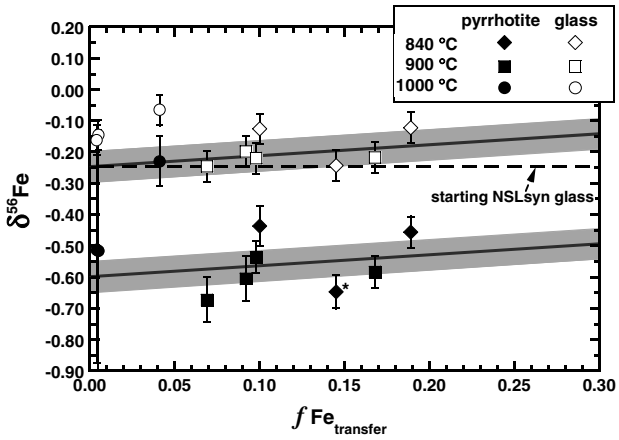

Fig. 5. δ^{56}Fe values of corresponding pyrrhotite (corrected for incomplete phase separation) and glass pairs from crystallisation experiments in comparison with calculated mass balance lines for equilibrium isotope fractionation in a closed system. Mass balance lines are constructed using the error weighted average of $\Delta^{56}Fe_{pyrrhotite\text{-}melt}$ of $-0.35‰$ obtained from crystallisation and isotope exchange experiments. The grey areas correspond to the analytical uncertainty ($\pm 0.049‰$) of δ^{56}Fe measurements. The pyrrhotite datum marked with an * represents the uncorrected measured δ^{56}Fe value (see Table 3).

4. Discussion

4.1. Stability of pyrrhotite

The stability field of pyrrhotite is a complex function of thermodynamic parameters, such as temperature, pressure, and the fugacity of sulphur and oxygen. From observations in natural samples and from experimental studies it is known that silicate melts can coexist with immiscible sulphide liquids from which sulphide minerals crystallise rapidly during cooling (Whitney, 1984; Luhr, 1990; Vaughan and Lennie, 1991; Clemente et al., 2004). Hence, to interpret the measured Fe isotope partitioning we have to consider whether pyrrhotite found in the run products was a stable phase at the experimental conditions or represents a quench phase.

As already described in Section 2.2.3 formation of a sulphur-rich liquid phase was observed for initial experiments with relatively high amounts of sulphur (up to 14.16 wt% S; Fig. 1A). This phase disappeared when the amount of sulphur was reduced (<0.53 wt% S) and pyrrhotite became the only sulphur-rich phase in the system (Fig. 1B–D). In crystallisation experiments pyrrhotite crystals are preferentially located at the former grain boundaries of the glass powder used as starting material (Fig. 1B) indicating heterogeneous nucleation of pyrrhotite under experimental conditions. If an immiscible sulphide liquid was present during the experiment, formation of a few larger pools is expected (to minimise surface energy), rather than numerous small droplets and even aggregates of droplets. Additional evidence that pyrrhotite is a stable phase at experimental conditions is given by the exchange experiments which show that the initially added pyrrhotite crystals were partly dissolved in the

silicate melt until sulphur and iron saturation was reached. These crystals show a typical dissolution texture (Fig. 1F). Their subhedral crystal shapes, however, are still preserved and no signs for formation of an immiscible sulphide liquid can be found.

4.2. Iron isotope fractionation

Both experimental approaches show that resolvable iron isotope fractionation exists at magmatic conditions. Pyrrhotite incorporates preferentially lighter Fe isotopes relative to the coexisting silicate melt. The fractionation factors determined from the crystallisation experiments are in good agreement with the values obtained from the isotope exchange experiments (Tables 2 and 3, Fig. 6). Understanding the mechanisms of isotope fractionation is necessary to interpret natural Fe isotope variations in igneous systems. In doing so, it is important to distinguish between kinetic and equilibrium fractionation. This issue will be discussed in the following section. Then we focus on the interpretation of the fractionation data in terms of structural and compositional parameters controlling the sign and magnitude of the Fe isotope fractionation factor by comparing the experimental data with predicted fractionations.

4.2.1. Kinetic or equilibrium isotope fractionation?

The two different experimental approaches (crystallisation and exchange experiments) follow two different reaction pathways. In the crystallisation experiments, Fe from the melt is transferred into pyrrhotite. Possible mechanisms controlling these experiments are diffusion of iron in the melt, reaction kinetics at the interfaces between sulphur/melt, pyrrhotite/sulphur and pyrrhotite/melt and diffusion of iron in the newly formed pyrrhotite. In the exchange experiments pyrrhotite is partly dissolved and controlling steps for the reaction may be diffusion of iron in the melt and in pyrrhotite, diffusion of sulphur into the melt and the interface reaction between pyrrhotite and melt.

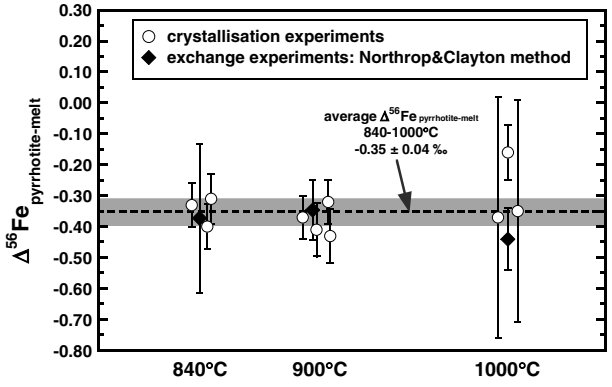

Fig. 6. Summary of the Fe isotope dataset obtained from the partial exchange experiments and the crystallisation experiments. The results of the crystallisation experiment agree well with those of the exchange experiment. Uncertainties associated with crystallisation experiments at 1000 °C are larger, due to higher uncertainties on the small changes in FeO_{total} (compare $f Fe_{transfer}$ in Table 3), which was used to correct the measured $\delta^{56}Fe$ of pyrrhotite for contamination with Fe from the glass during phase separation. The dashed line represents the error-weighted average of all $\Delta^{56}Fe_{pyrrhotite\text{-}melt}$ values from both the crystallisation experiments and the partial isotope exchange method.

There is no indication that interface reactions are important for the timescale required to achieve chemical and isotopic equilibrium in the system. Furthermore, diffusion of iron in pyrrhotite is very fast compared to the crystal sizes of pyrrhotite. According to Condit et al. (1974) the self diffusion coefficient D_{Fe} in $Fe_{0.9}S$ at 840 °C is 1.08×10^{-11} m^2/s. Hence, the timescale to equilibrate pyrrhotite crystals of 20 μm diameter is about 37 s, much lower than the experimental duration. In the crystallisation experiments the size of pyrrhotite crystals is much smaller and, hence, Fe isotopic equilibration of pyrrhotite is even faster. Thus, the mechanism which controls the equilibration of the samples is probably diffusion of iron in the melt. Experimental data for iron diffusion in the rhyolitic melts are not available, but data for lanthanum diffusion may serve as a lower limit for iron diffusion (La is in trivalent state whereas Fe is in a mixed divalent/trivalent state). At 800 °C and 500 MPa in rhyolitic melt containing 5 wt% water La-diffusivity is 6×10^{-15} m^2/s (Tegge-Schüring, 2003), resulting after 144 h run duration in a diffusion length ($\sqrt{(D \cdot t)}$) of 57 μm. This is similar to the average distance between pyrrhotite crystals. Diffusion in the more depolymerised and thus less viscous peralkaline melt at 840 °C can be expected to be significantly faster (Mungall, 2002). Hence, we conclude that iron diffusion in the melt is always fast enough to equilibrate iron isotopes in the sample during the applied run durations, consistent with the findings of the kinetic ^{57}Fe tracer experiments.

4.2.2. Effect of temperature on iron isotope fractionation

Equilibrium isotope fractionation typically shows a decrease in magnitude with increasing temperature with $1/T$ or $1/T^2$ (Urey, 1947). However, predicted changes of the fractionation factors for any mineral combination in the investigated temperature range between 840 and 1000 °C (Polyakov and Mineev, 2000) are below analytical resolution. Indeed, our experiments did not reveal any temperature dependence of the fractionation factor within experimental and analytical precision (Fig. 6). However, an alternative explanation for the lack of temperature dependence is that the fractionation measured in the quenched phases is overprinted by retrograde exchange processes. Thus it has to be discussed whether the data reflect equilibrium at high temperature or the isotopic closure temperature of the system (Dodson, 1973). As discussed above Fe diffusion in the silicate melt is probably the limiting factor controlling equilibration. Thus, although Fe re-equilibration by diffusion within a pyrrhotite crystal might be possible during quenching, an isotope exchange between pyrrhotite and silicate melt would be limited by the Fe diffusivity in the silicate melt. The typical time to cool the experimental charges from the run temperature

to 400 °C (at this temperature cation diffusion in the melt can be considered as essentially frozen-in) was less than 3 min. As shown in Fig. 3 this time interval is very short compared to the characteristic equilibration time of >24 h at 900 °C. At lower temperature the equilibration time is even longer. Thus, we conclude that only a minor fraction of iron isotopes can exchange during cooling and the measured fractionation factors reflect the near-equilibrium fractionation under the given experimental conditions.

We propose an average fractionation factor between pyrrhotite and silicate melt of $\Delta^{56}Fe_{pyrrhotite\text{-}melt} = -0.35 \pm 0.04‰$ (2SE, $n = 13$) at 500 MPa and temperatures between 840 and 1000 °C. This value represents the error-weighted average of all fractionation data from the exchange experiments using the method of Northrop and Clayton (1966) and the crystallisation experiments (Tables 2 and 3) and was calculated using the *Isoplot* program (Ludwig, 2001). The given uncertainty ($2SE = t \cdot \frac{\sigma}{\sqrt{n}}$) describes the 95% confidence level for the mean value of the population, with $n = 13$ and a Student's t factor of $t = 2.18$ for 12 degrees of freedom at the 95% confidence level.

4.3. Mechanisms of isotope fractionation

To develop insights into the mechanisms of Fe isotope fractionation between pyrrhotite and silicate melt, we compare our results to predictions based on Mössbauer spectroscopy data (Polyakov and Mineev, 2000) (Fig. 7). Currently, no predictions of Fe isotope fractionation between minerals and silicate melts are available. Therefore, we assume that the reduced isotopic partition function ratios (β-factors) of ferrous and ferric iron bearing silicate minerals can be used as reasonable approximations of

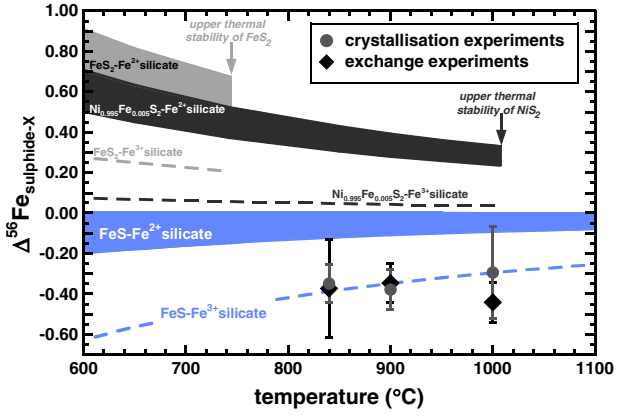

Fig. 7. Experimentally determined Fe isotope fractionation between pyrrhotite ($Fe_{1-x}S$) and rhyolitic melt. Also plotted are the predicted equilibrium isotope fractionations between sulphide minerals and ferric or ferrous Fe dominated silicate minerals, calculated on the basis of Mössbauer and INRXS data by Polyakov and Mineev (2000) and Polyakov (2006, personal communication). Thermal stability limits valid for 1 atm (Craig and Scott, 1974).

β-factors for silicate melts. For ferric iron-dominated silicates we used the β-factor of aegirine (Polyakov and Mineev, 2000). The ferrous iron silicate "fields" shown in Fig. 7 were calculated on the basis of the entire range of β-factors available for olivine, diopside, enstatite and hedenbergite from Polyakov and Mineev (2000). The β-factors of FeS_2 and $Ni_{0.995}Fe_{0.005}S_2$ are also from Polyakov and Mineev (2000). The β-factor of FeS (troilite) was calculated by Polyakov (2006, personal communication) following the method described in Polyakov et al. (2005) on the basis of the partial phonon density of state (PDOS), obtained by inelastic nuclear resonant X-ray scattering (INRXS) at 1.5 GPa by Kobayashi et al. (2004). The stoichiometric polymorph of FeS, troilite, that is stable only up to about 140 °C at 1 atm (Craig and Scott, 1974), differs from high-temperature hexagonal pyrrhotite only by a slight distortion from the ideal NiAs structure. The NiAs structure type exhibits considerable chemical flexibility due to accommodation of metal vacancies, common for pyrrhotites. Thus, we conclude that the β-factor of FeS (troilite) can be considered as representative for pyrrhotite in our experimental temperature range.

Our experimental findings are consistent with the predicted Fe isotope fractionation between FeS and a ferric iron dominated silicate (Fig. 7), suggesting that the Fe redox state in the silicate melt plays an important role for Fe isotope fractionation. Our experimentally determined fractionation factor is representative for a specific $Fe^{2+}/\Sigma Fe$ ratio (0.38 ± 0.02). From Fig. 7 it is evident that if the silicate melt becomes more reduced, a decrease in the fractionation factor between pyrrhotite and silicate melt is predicted, perhaps approaching zero.

Differences in coordination of Fe exists between pyrrhotite and the silicate melt present in our experiments that may affect Fe isotope fractionation as well (Schauble, 2004). Contrary to pyrrhotite, the peralkaline melt contains both ferric and ferrous iron. Ferric iron is predominantly tetrahedrally coordinated by oxygen. However, some Fe^{3+} may also be present in five- or six-fold coordination (Mysen and Richet, 2005). The coordination of Fe^{2+} in silicate melts is still debated. A continuous distribution of Fe^{2+} environments from four-fold to six-fold coordination in silicate melts has been suggested (e.g., Seifert et al., 1979; Virgo and Mysen, 1985; Rossano et al., 2000; Farges et al., 2004; Wilke et al., 2006). However, for silica-rich melts it can be expected that most Fe^{2+} is octahedrally coordinated (e.g., Mysen et al., 1982; Virgo and Mysen, 1985). Given that all other parameters are identical one might expect an enrichment of the heavier isotopes in the phase where Fe has a lower coordination number (Schauble, 2004). In our experiments octahedrally coordinated Fe in pyrrhotite is isotopically lighter than the silicate melt with primarily tetrahedrally coordinated Fe (possibly along with minor Fe in five- and six-fold coordination), which is consistent with theory.

Moreover, it can be seen from Fig. 7, that considerable differences in isotope fractionation exist between the differ-

ent Fe sulphides. For example, a change of the sign of the fractionation factor occurs comparing FeS with FeS_2 and $Ni_{0.995}Fe_{0.005}S_2$, although all three sulphides contain octahedrally coordinated ferrous Fe. Hence, there must be other factors governing Fe isotope fractionation besides the valency and the coordination of Fe. A possible explanation may lie in the nature of bonding in the sulphides and the related electron-configuration. In pyrrhotite iron is in the high-spin state (Prewitt and Rajamani, 1974), i.e., four of the six 3d electrons occupy the three t_{2g} orbitals, forming only one π bond. Additionally, a metallic Fe–Fe bond along the *c*-axis of the NiAs cell is present in the pyrrhotite structure, although it is subsidiary to the main Fe–S bond (e.g., Tokonami et al., 1972; Farrell and Fleet, 2001). On the other hand in the pyrite-type sulphides iron is in the low spin-state (Prewitt and Rajamani, 1974), i.e., all six 3d electrons fill the three t_{2g} orbitals, forming three π bonds. This π bond formation increases the covalency of the Fe–S bond in the sequence $FeS < Ni_{1-x}Fe_xS_2 < FeS_2$ (Prewitt and Rajamani, 1974), consistent with the sequence of the respective β-factors (Fig. 7). This highlights the importance of the bond character as an influencing factor on inter-mineral Fe isotope fractionation, as already emphasised by Polyakov and Mineev (2000) and Schauble (2004).

For our experiments, we suggest that differences in ligands and Fe redox state (to which Fe coordination is linked) between pyrrhotite and silicate melt most likely control the sign and magnitude of isotope fractionation.

4.4. Applications to natural systems—perspectives

Pyrrhotite ($Fe_{1-x}S$) is a common iron sulphide and an important constituent of ore deposits. It is also found in pegmatites, in contact metamorphic deposits, in high temperature metamorphic veins and in sediments. Pyrrhotite has repeatedly been observed in mafic and felsic magmatic environments as an accessory mineral phase and as inclusions within phenocrysts (e.g., Ueda and Itaya, 1981; Whitney and Stormer, 1983; Vaughan and Lennie, 1991). Natural pyrrhotites, like other sulphides such as pyrite and chalcopyrite (Graham et al., 2004; Rouxel et al., 2004), show a considerable range in Fe isotope compositions. For example the pyrrhotite samples analysed in this study cover a range from −1.04‰ to −0.37‰ in δ^{56}Fe (Table 1), while the mean mafic Earth has a δ^{56}Fe value of +0.069‰ (re-calculated from the δ^{57}Fe values reported by Poitrasson et al., 2004). If we consider the fractionation factor between pyrrhotite and ferric iron-rich peralkaline rhyolitic melt of $\Delta^{56}Fe_{pyrrhotite\text{-}melt} = -0.35‰$ as a maximum value at magmatic temperatures, then primary pyrrhotites of igneous origin are expected to have δ^{56}Fe values that are only slightly lower than or even equal to that of the mean mafic Earth. Consequently, the very negative δ^{56}Fe values of some pyrrhotites (Table 1) cannot be explained solely by primary magmatic mineral-melt fractionation. Other processes, such as hydrothermal activity and metamorphism or other isotopically fractionated Fe sources need to be involved in pyrrhotite formation to explain these values. Hence, Fe isotope systematics may be a useful tool to determine the origin and evolution of sulphide ore deposits.

Another interesting aspect arises from the conclusion that the redox state of iron plays an important role on the Fe isotope fractionation in magmatic systems. In natural silicate melts a high variability of the redox state of Fe exists depending on the magma composition. On average the $Fe^{2+}/\Sigma Fe$ decreases as magmatic liquids become more felsic (e.g., Mysen, 1988; Fig. 8.19). Our experimentally determined fractionation factor probably represents an upper limit for iron isotope fractionation during pyrrhotite crystallisation from magmas in nature. A much smaller fractionation (probably approaching zero) than in our experiments can be expected for a MORB system, with $Fe^{2+}/\Sigma Fe$ ratios of silicate melts typically >0.8 (e.g., Bezos and Humler, 2005). Considering the variations in oxygen fugacity found in natural magmatic systems with different chemical compositions, and the related diversity in the redox state of Fe in silicate melts, a variation of mineral-melt Fe isotope fractionation in general is likely, assuming a sensitivity of the fractionation factor to the Fe redox state. If true, Fe isotopes may serve as a tracer for changing redox conditions in magmatic systems. However, a prerequisite to this application would be that the change in mineral-melt fractionation as a function of the $Fe^{2+}/\Sigma Fe$ ratio of the melt is analytically resolvable. Up to date no such studies have been done and further investigation is needed.

5. Conclusions

The experimentally studied Fe isotope partitioning between coexisting iron sulphide (pyrrhotite) and a hydrous rhyolitic melt at magmatic conditions (840 to 1000 °C, 500 MPa) show that pyrrhotite preferentially incorporates lighter Fe isotopes relative to silicate melt. For the investigated temperature range from 840 to 1000 °C we determined an average equilibrium Fe isotope fractionation factor of $\Delta^{56}Fe_{pyrrhotite\text{-}melt} = -0.35 \pm 0.04‰$ (2SE, $n = 13$). In comparison to the relatively ferric iron-rich peralkaline rhyolitic composition used in our experiments a smaller Fe isotope fractionation factor is expected between pyrrhotite and a basaltic melt with a higher $Fe^{2+}/\Sigma Fe$ ratio.

Ferrous iron bonded to sulphur in pyrrhotite forms a marked contrast in comparison to oxygen-coordinated Fe in a mixed divalent/trivalent state in the silicate melt (i.e., [Fe(II)–S] in pyrrhotite vs. [Fe(II)/Fe(III)–O] in the silicate melt). Thus, in view of the high temperatures the relatively large isotope fractionation determined in this study is most likely a consequence of significant differences in the redox state and in the ligand of Fe between the phases. This might explain why Fe isotope fractionation observed between silicate minerals in igneous rocks (e.g., Beard and

Johnson, 2004), where Fe is solely coordinated by oxygen, is smaller or not resolvable at all.

Acknowledgments

We express our thanks to F. Melcher and U. Vetter (BGR: German Geological Survey) for providing natural pyrrhotite samples and for fruitful discussions regarding sulphide ore formation processes. We are also grateful to the Mineralogical Museum, University of Köln (R. Hollerbach, I. Kerkamm) for kindly providing the pyrrhotite sample K. O. Diedrich is acknowledged for preparation of the thin sections. We are greatly indebted to V. Polyakov for generously providing us with unpublished β-factor data of troilite and for fruitful discussion of sulphide β-factors in general. We also thank T. Gesing for his assistance with XRD measurements. A. Tangen, C. Thürnagel and A. Wegorzewski are thanked for their assistance in the laboratory. Thanks to K. Norton for linguistic improvement of the manuscript. We gratefully acknowledge financial support by the German Research Foundation (DFG) Grant SCHO-1071. We thank E. Schauble, F. Poitrasson, two anonymous reviewers and Associate Editor C. M. Johnson for their thoughtful and constructive reviews that significantly helped to improve the quality of the manuscript.

Associate editor: Clark M. Johnson

Appendix A. Supplementary data

Supplementary data associated with this article can be found, in the online version, at doi:10.1016/j.gca.2006.09.012.

References

Beard, B.L., Johnson, C.M., 2004. Inter-mineral Fe isotope variations in mantle-derived rocks and implications for the Fe geochemical cycle. *Geochim. Cosmochim. Acta* **68** (22), 4727–4743.

Beard, B.L., Johnson, C.M., Skulan, J.L., Nealson, K.H., Cox, L., Sun, H., 2003. Application of Fe isotopes to tracing the geochemical and biological cycling of Fe. *Chem. Geol.* **195** (1–4), 87–117.

Behrens, H., Jantos, N., 2001. The effect of anhydrous composition on water solubility in granitic melts. *Am. Mineral.* **86** (1–2), 14–20.

Behrens, H., Stuke, A., 2003. Quantification of H_2O contents in silicate glasses using IR spectroscopy—a calibration based on hydrous glasses analyzed by Karl-Fischer titration. *Glass Sci. Technol.* **76** (4), 176–189.

Berndt, J., Koepke, J., Holtz, F., 2005. An experimental investigation of the influence of water and oxygen fugacity on differentiation of MORB at 200 MPa. *J. Petrol.* **46** (1), 135–167.

Berndt, J., Liebske, C., Holtz, F., Freise, M., Nowak, M., Ziegenbein, D., Hurkuck, W., Koepke, J., 2002. A combined rapid-quench and H_2-membrane setup for internally heated pressure vessels: description and application for water solubility in basaltic melts. *Am. Mineral.* **87**, 1717–1726.

Bezos, A., Humler, E., 2005. The $Fe^{3+}/\Sigma Fe$ ratios of MORB glasses and their implications for mantle melting. *Geochim. Cosmochim. Acta* **69** (3), 711–725.

Botcharnikov, R.E., Behrens, H., Holtz, F., Koepke, J., Sato, H., 2004. Sulfur and chlorine solubility in Mt. Unzen rhyodacitic melt at 850 °C and 200 MPa. *Chem. Geol.* **213** (1-3), 207–225.

Clemente, B., Scaillet, B., Pichavant, M., 2004. The solubility of sulphur in hydrous rhyolitic melts. *J. Petrol.* **45** (11), 2171–2196.

Cole D.R., Chakraborty, S,. 2001. Rates and mechanisms of isotopic exchange. In: *Stable Isotope Geochemistry—Reviews in Mineralogy and Geochemistry*, vol. 43. Mineralogical Society of America, Washington, pp. 83–223.

Condit, R.H., Hobbins, R.R., Birchenall, C.E., 1974. self-diffusion of iron and sulfur in ferrous sulfide. *Oxid. Met.* **8** (6), 409–455.

Craig J.R., Scott, S.D., 1974. Sulfide phase equilibria. In: *Sulfide Mineralogy—Reviews in Mineralogy*, vol. 1., Mineralogical Society of America, CS 1–104.

Criss, R.E., Gregory, R.T., Taylor, H.P., 1987. kinetic-theory of oxygen isotopic exchange between minerals and water. *Geochim. Cosmochim. Acta* **51** (5), 1099–1108.

Criss, R.E., 1999. *Principles of stable isotope distribution*. Oxford University Press, Oxford.

Dauphas, N., Rouxel, O., 2006. Mass spectrometry and natural variations of iron isotopes. *Mass Spectrom. Rev.* **25** (4), 515–550.

Devine, J.D., Gardner, J.E., Brack, H.P., Layne, G.D., Rutherford, M.J., 1995. Comparison of microanalytical methods for estimating H_2O contents of silicic volcanic glasses. *Amer. Mineral.* **80** (3–4), 319–328.

Dickenson, M.P., Hess, P.C., 1986. The structural role and homogeneous redox equilibria of iron in peraluminous, metaluminous and peralkaline silicate melts. *Contrib. Mineral. Petr.* **92** (2), 207–217.

Dodson, M.H., 1973. Closure temperature in cooling geochronological and petrological systems. *Contrib. Mineral. Petr.* **40** (3), 259–274.

Farges, F., Lefrere, Y., Rossano, S., Berthereau, A., Calas, G., Brown, G.E., 2004. The effect of redox state on the local structural environment of iron in silicate glasses: a molecular dynamics, combined XAFS spectroscopy, and bond valence study. *J. Non-Cryst. Solids* **344** (3), 176–188.

Farrell, S.P., Fleet, M.E., 2001. Sulfur K-edge XANES study of local electronic structure in ternary monosulfide solid solution (Fe, Co, Ni) (0.923)S. *Phys. Chem. Miner.* **28** (1), 17–27.

Gaillard, F., Scaillet, B., Pichavant, M., 2002. Kinetics of iron oxidation–reduction in hydrous silicic melts. *Am. Mineral.* **87** (7), 829–837.

Gaillard, F., Scaillet, B., Pichavant, M., Beny, J.L., 2001. The effect of water and $fO(2)$ on the ferric–ferrous ratio of silicic melts. *Chem. Geol.* **174** (1–3), 255–273.

Graham, S., Pearson, N., Jackson, S., Griffin, W., O'Reilly, S.Y., 2004. Tracing Cu and Fe from source to porphyry: in situ determination of Cu and Fe isotope ratios in sulfides from the Grasberg Cu–Au deposit. *Chem. Geol.* **207** (3–4), 147–169.

Johnson, C.M., Skulan, J.L., Beard, B.L., Sun, H., Nealson, K.H., Braterman, P.S., 2002. Isotopic fractionation between Fe(III) and Fe(II) in aqueous solutions. *Earth Planet. Sci. Lett.* **195** (1-2), 141–153.

Johnson, C.M., Beard, B.L., Albarede, F., (Eds.), 2004. Geochemistry of non-traditional stable isotopes, Rev. Mineral. Geochem. vol. 55. Mineralogical Society of America, Washington, p. 454.

Kobayashi, H., Kamimura, T., Alfe, D., Sturhahn, W., Zhao, J.Y., Alp, E.E., 2004. Phonon density of states and compression behavior in iron sulfide under pressure. *Phys. Rev. Lett.* **93** (19), 1955031–1955034.

Leschik, M., Heide, G., Frischat, G.H., Behrens, H., Wiedenbeck, M., Wagner, N., Heide, K., Geissler, H., Reinholz, U., 2004. Determination of H_2O and D_2O contents in rhyolitic glasses. *Phys. Chem. Glasses* **45** (4), 238–251.

Ludwig, K.R., 2001. Isoplot—A Geochronological Toolkit for Microsoft Excel, Version 2.49. Berkeley Geochronology Center Special Publication, No. 1a, p. 55.

Luhr, J.F., 1990. Experimental phase-relations of water-saturated and sulfur-saturated Arc Magmas and the 1982 eruptions of El-Chichon volcano. *J. Petrol.* **31** (5), 1071–1114.

Mills, G.A., Urey, H.C., 1940. The kinetics of isotopic exchange between carbon dioxide, bicarbonate ion, carbonate ion and water. *J. Am. Chem. Soc.* **62**, 1019–1026.

Morgan, G.B., London, D., 1996. Optimizing the electron microprobe analysis of hydrous alkali aluminosilicate glasses. *Am. Mineral.* **81** (9–10), 1176–1185.

Mungall, J.E., 2002. Empirical models relating viscosity and tracer diffusion in magmatic silicate melts. *Geochim. Cosmochim. Acta* **66**, 125–143.

Mysen, B.O., 1988. *Structure and Properties of Silicate Melts*. Elsevier, Amsterdam.

Mysen, B.O., Richet, P., 2005. Silicate glasses and melts—properties and structure. *Dev. Geochem.* **10**, 544.

Mysen, B.O., Virgo, D., Seifert, F.A., 1982. The structure of silicate melts—implications for chemical and physical-properties of natural magma. *Rev. Geophys.* **20** (3), 353–383.

Northrop, D.A., Clayton, R.N., 1966. oxygen-isotope fractionations in systems containing dolomite. *J. Geol.* **74** (2), 174–196.

Poitrasson, F., Freydier, R., 2005. Heavy iron isotope composition of granites determined by high resolution MC-ICP-MS. *Chem. Geol.* **222** (1–2), 132–147.

Poitrasson, F., Halliday, A.N., Lee, D.C., Levasseur, S., Teutsch, N., 2004. Iron isotope differences between Earth, Moon, Mars and Vesta as possible records of contrasted accretion mechanisms. *Earth Planet. Sci. Lett.* **223** (3–4), 253–266.

Polyakov, V.B., Mineev, S.D., 2000. The use of Mössbauer spectroscopy in stable isotope geochemistry. *Geochim. Cosmochim. Acta* **64** (5), 849–865.

Polyakov, V.B., Mineev, S.D., Clayton, R.N., Hu, G., Mineev, K.S., 2005. Determination of tin equilibrium isotope fractionation factors from synchrotron radiation experiments. *Geochim. Cosmochim. Acta* **69** (23), 5531–5536.

Prewitt, C.T., Rajamani, V., 1974. Electron interactions and chemical bonding in sulfides. In: *Sulfide Mineralogy—Reviews in Mineralogy*, vol. 1. Mineralogical Society of America, PR 1–41.

Rossano, S., Ramos, A., Delaye, J.M., Creux, S., Filipponi, A., Brouder, C., Calas, G., 2000. EXAFS and molecular dynamics combined study of CaO–FeO–2SiO(2) glass. New insight into site significance in silicate glasses. *Europhys. Lett.* **49** (5), 597–602.

Rouxel, O., Fouquet, Y., Ludden, J.N., 2004. Subsurface processes at the Lucky Strike hydrothermal field, Mid-Atlantic Ridge: evidence from sulfur, selenium, and iron isotopes. *Geochim. Cosmochim. Acta* **68** (10), 2295–2311.

Schauble, E.A., 2004. Applying stable isotope fractionation theory to new systems. In: *Reviews in Mineralogy and Geochemistry—Geochemistry of Non-Traditional Stable Isotopes*, vol. 55, pp. 65–111.

Schoenberg, R., von Blanckenburg, F., 2005. An assessment of the accuracy of stable Fe isotope ratio measurements on samples with organic and inorganic matrices by high-resolution multicollector ICP-MS. *Int. J. Mass Spectrom.* **242** (2–3), 257–272.

Seifert, F., Virgo, D., Mysen, B.O., 1979. Melt structures and redox equilibria in the system Na_2O–FeO–Fe_2O_3–Al_2O_3–SiO_2. *Carnegie Institution Washington Yearbook* **78**, 511–519.

Tamic, N., Behrens, H., Holtz, F., 2001. The solubility of H_2O and CO_2 in rhyolitic melts in equilibrium with a mixed CO_2–H_2O fluid phase. *Chem. Geol.* **174** (1–3), 333–347.

Tegge-Schüring, A.S., 2003. Cation Diffusion in Silicate Melts. Ph.D. thesis, University of Hannover.

Tokonami, M., Nishiguc, K., Morimoto, N., 1972. crystal-structure of a monoclinic pyrrhotite (Fe_7S_8). *Am. Mineral.* **57** (7–8), 1066–1080.

Ueda, A., Itaya, T., 1981. Microphenocrystic pyrrhotite from dacite rocks of Satsuma-Iwojima, Southwest Kyushu, Japan and the solubility of sulfur in dacite magma. *Contrib. Mineral. Petr.* **78** (1), 21–26.

Urey, H.C., 1947. The thermodynamic properties of isotopic substances. *J. Chem. Soc.*, 562–581.

Vaughan, D.J., Craig, J.R., 1978. *Mineral Chemistry of Metal Sulfides*. University Press, Cambridge.

Vaughan, D.J., Lennie, A.R., 1991. The iron sulfide minerals—their chemistry and role in nature. *Sci. Prog.* **75** (298), 371–388.

Virgo, D., Mysen, B.O., 1985. The structural state of iron in oxidized vs reduced glasses at 1 atm—a Fe-57 Mossbauer Study. *Phys. Chem. Miner.* **12** (2), 65–76.

Welch, S.A., Beard, B.L., Johnson, C.M., Braterman, P.S., 2003. Kinetic and equilibrium Fe isotope fractionation between aqueous Fe(II) and Fe(III). *Geochim. Cosmochim. Acta* **67** (22), 4231–4250.

Weyer, S., Anbar, A.D., Brey, G.P., Munker, C., Mezger, K., Woodland, A.B., 2005. Iron isotope fractionation during planetary differentiation. *Earth Planet. Sci. Lett.* **240** (2), 251–264.

Whitney, J.A., 1984. Fugacities of sulfurous gases in pyrrhotite-bearing silicic magmas. *Am. Mineral.* **69** (1–2), 69–78.

Whitney, J.A., Stormer, J.C., 1983. Igneous sulfides in the Fish Canyon Tuff and the role of sulfur in calc-alkaline magmas. *Geology* **11** (2), 99–102.

Wilke, M., Schmidt, C., Farges, F., Malavergne, V., Gautron, L., Simionovici, A., Hahn, M., Petit, P.E., 2006. Structural environment of iron in hydrous aluminosilicate glass and melt—evidence from X-ray absorption spectroscopy. *Chem. Geol.* **229** (1–3), 144–161.

Williams, H.M., McCammon, C.A., Peslier, A.H., Halliday, A.N., Teutsch, N., Levasseur, S., Burg, J.P., 2004. Iron isotope fractionation and the oxygen fugacity of the mantle. *Science* **304** (5677), 1656–1659.

Williams, H.M., Peslier, A.H., McCammon, C., Halliday, A.N., Levasseur, S., Teutsch, N., Burg, J.P., 2005. Systematic iron isotope variations in mantle rocks and minerals: the effects of partial melting and oxygen fugacity. *Earth Planet. Sci. Lett.* **235** (1–2), 435–452.

Wilson, A.D., 1960. The micro-determination of ferrous iron in silicate minerals by a volumetric and colorimetric method. *Analyst* **85**, 823–827.

York, D., 1969. Least squares fitting of a straight line with correlated errors. *Earth Planet. Sci. Lett.* **5**, 320–324.

Zhu, X.K., Guo, Y., Williams, R.J.P., O'Nions, R.K., Matthews, A., Belshaw, N.S., Canters, G.W., de Waal, E.C., Weser, U., Burgess, B.K., Salvato, B., 2002. Mass fractionation processes of transition metal isotopes. *Earth Planet. Sci. Lett.* **200** (1–2), 47–62.